Since January 2020 Elsevier has created a COVID-19 resource centre with free information in English and Mandarin on the novel coronavirus COVID-19. The COVID-19 resource centre is hosted on Elsevier Connect, the company's public news and information website.

Annals of Diagnostic Pathology 61 (2022) 152032

Contents lists available at ScienceDirect

Annals of Diagnostic Pathology

journal homepage: www.elsevier.com/locate/anndiagpath

Original Contribution

The differential immune response in mild versus fatal SARS-CoV2 infection☆

David Suster [a], Esmerina Tili [b], Gerard J. Nuovo [c,d,*]

[a] Rutgers University Hospital Department of Pathology, Newark, NJ, USA
[b] The Ohio State University Wexner Medical Center, Department of Anesthesiology, College of Medicine, Columbus, OH, USA
[c] The Ohio State University Comprehensive Cancer Center, Columbus, OH, USA
[d] GnomeDX, Powell, OH, USA

ARTICLE INFO

Keywords:
COVID-19
SARS-CoV2
Mild disease
Fatal disease
Immune response

ABSTRACT

This study compared the immune response in mild versus fatal SARS-CoV2 infection. Forty nasopharyngeal swabs with either productive mild infection (n = 20) or negative for SARS-CoV2 (n = 20) were tested along with ten lung sections from people who died of COVID-19 which contained abundant SARS-CoV2 and ten controls. There was a 25-fold increase in the CD3+T cell numbers in the viral positive nasopharyngeal swabs compared to the controls ($p < 0.001$) and no change in the CD3+T cell count in the fatal COVID-19 lungs versus the controls. CD11b + and CD206+ macrophage counts were significantly higher in the mild versus fatal disease ($p = 0.002$). In situ analysis for SARS-CoV2 RNA found ten COVID-19 lung sections that had no/rare detectable virus and also lacked the microangiopathy typical of the viral positive sections. These viral negative lung tissues when compared to the viral positive lung samples showed a highly significant increase in CD3+ and CD8 T cells ($p < 0.001$), equivalent numbers of CD163+ cells, and significantly less PDL1, CD11b and CD206+ cells ($p = 0.002$). It is concluded that mild SARS-CoV2 infection is marked by a much stronger CD3/CD8 T cell, CD11b, and CD206 macrophage response than the fatal lung disease where viral RNA is abundant.

1. Introduction

The COVID-19 pandemic has of this writing infected over 600 million people with >6 million deaths. Most people infected with SARS-CoV2 have a mild clinical course. The majority of people who die of the disease, about 1–2 % of the total, are over 65 years old and have co-morbidities that include obesity, diabetes, and/or cardiovascular disease amongst others [1,2]. This clinical observation raises a key question: is there a difference in the immune response to the virus in the approximately 85 % of people who do not require hospitalization (mild disease) versus those whom require hospitalization or die of the disease (severe disease) This question has been addressed mostly by sera-based studies that have compared the immune profile in mild versus severe SARS-CoV2 infections. Such studies have indicated that increased FOXP3+ T regulatory cells and reduced CD3+/CD8+ cytotoxic cells in the sera is associated with worse clinical outcomes [3-5]. To our knowledge, no such comparative in situ based study has been done using samples from the two main sources of productive infection by SARS-CoV2, the nasopharynx and the lung.

SARS-CoV2 RNA and its associated nucleocapsid plus spike proteins are found in high copy number in the nasopharynx of people with mild infection as well as in the lung of people who died of COVID-19 [6-8]. The data regarding infectious SARS-CoV2 in other organs is diverse, with several papers indicating that infectious virus can also be found in many sites including the blood, placenta, brain, and heart [9-12]. This has led some to hypothesize that severe/fatal COVID-19 represents systemic infection that often involves the endothelial cells of microvessels [9-12]. However, other publications have refuted this idea and documented that the viral spike protein per se can be cytotoxic and capable of generating the cytotoxic storm and hypercoagulable state typical of fatal COVID-19 [7,13-15].

The purpose of this study was to collect a series of nasopharyngeal swabs from people documented to have mild SARS-CoV2 infection by qRTPCR/clinical history and compare the immune response to lung samples of people who died of COVID-19 and to the relevant controls in a blinded fashion. Also, since the lung samples from people who died of

☆ Financial support: OSU Dept of Anesthesiology bridge fund (ET).
* Corresponding author at: 1476 Manning Parkway, Powell, OH, USA.
E-mail address: nuovo.1@osu.edu (G.J. Nuovo).

https://doi.org/10.1016/j.anndiagpath.2022.152032

Available online 2 September 2022

COVID-19 showed marked heterogeneity with regards to SARS-CoV2 viral load, we compared ten tissues with very high viral load to ten COVID-19 lung samples with rare/no detectable virus for the immune response and the H&E findings. Nasopharyngeal samples from people with fatal COVID-19 were not available for study. However, since the nasopharynx shows high copy infectious SARS-CoV2 in people with mild disease (8), comparing the immune response to the lung (fatal) and nasopharynx (mild) has the common variable of the host's response to a high viral load.

2. Materials and methods

2.1. COVID-19 autopsies, nasopharyngeal swabs, and controls

Autopsy material from the lung was available from fourteen people who died of COVID-19. Ten lung tissues from eight aged matched patients who died prior to 2016 served as negative controls. Five of these control lung tissues were the normal tissue adjacent to cancer and, in each case, the lung tissue was described as unremarkable. The 40 nasopharyngeal swabs were obtained from people being tested for SARS-CoV2 RNA by qRTPCR in an out-patient clinic setting set up specifically for COVID-19 testing with samples stored at 4C.

2.2. Immunohistochemistry

Immunohistochemistry was done as previously reported [16-18]. In brief, the Leica Bond Max automated platform with both the Fast red (DS 9820) and the DAB (DS 9800) detection kits (Leica Biosystems, Buffalo Grove, IL) were used with equivalent results. SARS-CoV2 specific antibodies against nucleocapsid (catalogue #9099), spike subunit 1 (#9083), and spike subunit 2 (#9123) were from ProSci (Poway, CA). The host response was analyzed with antibodies against CD3, CD8, CD20, CD41, FOXP3, fibrinogen, the macrophage markers CD11b, CD163, and CD206, as well as PDL1, IL6, TNFα, complement terminal complex C5b-9, and complement component 6 (C6). The HRP conjugate from Enzo Life Sciences (Farmingdale, New York, USA) was used in cases in place of the equivalent reagent from Leica in the DAB kit as this has been shown to reduce background [18].

2.3. In situ hybridization

Detection of SARS-CoV-2 RNA was done using the ACD RNAscope (Newark, California, USA) probe (Cat No. 848561-C3) following the manufacturers recommended protocol as previously published [7,8,16,17].

2.4. Co-expression and statistical analyses

The number of positive cells/200× field was counted with the InForm software or manually in 10 fields/tissue blinded to the SARS-CoV2 and clinical data. Statistical analysis was done using the InStat Statistical Analysis Software (version 3.36) and a paired *t*-test (also referred to as a "repeated measure t-test"). The null hypothesis was rejected if the significance level was below 5 %.

Co-expression analyses were done using the Nuance/InForm system whereby each chromogenic signal is separated, converted to a fluorescence-based signal, then mixed to determine the percentage of co-localization as previously described [7,8,16,17].

3. Results

3.1. Clinical/pathologic correlation

Autopsy material including the lungs was available from fourteen patients who died of COVID-19; the lung sections were taken from areas of lung consolidation. They ranged in age from 50 to 79 (mean 66) with seven men and seven women. In situ SARS-CoV2 analyses identified 10 lung tissues with very high viral load. These were compared to ten lung tissues from eight aged matched controls that were histologically unremarkable samples obtained prior to the COVID-19 pandemic. The most common co-morbidities in the COVID-19 patients were: hypertensive cardiomegaly (10/14), type II diabetes mellitus (9/14), chronic renal disease (often associated with diabetes) (8/14), and obesity (11/14). Multi-organ failure was documented in 9/14 patients. The length of time from diagnosis of SARS-CoV2 infection until death ranged from 3 to 22 days (mean 12.5 days). None of the patients were on chemotherapy, although two were on immunosuppressive medication for organ transplantation, and none received monoclonal antibodies versus viral spike protein.

The 40 nasopharyngeal swabs were obtained from people being tested for SARS-CoV2 RNA by qRTPCR in an out-patient clinic setting who ranged in age from 25 to 72 (mean 39) and had either no or mild symptoms (anosmia, nasal discharge, and/or low grade fever) for 1 to 5 days. Information about vaccine status was not available. Twenty of the samples were SARS-CoV2 positive (low CT counts = high viral copy number) and served as the cases whereas the other 20 were viral negative and served as the controls.

3.2. In situ hybridization for SARS-CoV2 RNA

Initially each of the lung samples (ten controls and twenty COVID-19 lung tissues from fourteen patients) were tested for SARS-CoV2 RNA by in situ hybridization blinded to the clinical information. Each of the controls was negative (Fig. 1A). COVID-19 lung tissues were separated into "high viral copy number" and "not viral associated" based on the amount of SARS CoV2 RNA identified by in situ hybridization. High viral copy number was defined by at least 33 % of the lung area containing SARS-CoV2 RNA (Fig. 1B). The SARS-CoV2 proteins (nucleocapsid, spike subunits S1 and S2) were found in the same distribution as the viral RNA (Fig. 1C). "Not viral associated" was defined by either no viral RNA detection or <5 % of the lung area containing viral RNA. Of the twenty lung tissues from patients that died of COVID-19, ten showed "high viral copy" and the other ten were classified as "not viral associated"; in several cases high viral copy and not viral associated lung tissues were from different lobes in the same person.

The forty nasopharyngeal swabs were next tested for SARS-CoV2 RNA by in situ hybridization blinded to the qRTPCR data. There was 100 % concordance between the qRTPCR and SARS-CoV2 RNA in situ hybridization data. Viral load was determined from the signal intensity and the percentage of target cells positive for viral RNA; in the nasopharynx SARS-CoV2 infects glandular cells [8]. By combining an immunohistochemistry test for epithelial membrane antigen, which marks glandular cells, with the cytologic features of glandular cells, it was determined that the mean percentage of glandular cells in the positive nasopharyngeal swabs was 22.3 %. The range of SARS-CoV2 positive cells in the swabs was 11.3 to 26.1 % (mean 16.2 %). The signal intensity in each case was, as in the lungs, 3+. Thus, the viral positive swabs were also classified as high viral copy number since on average over 50 % of the target cell contained a 3+ signal which has been estimated to correspond to several hundred viral copies per infected cell [16].

3.3. Immunohistochemistry for viral proteins

In order to corroborate the SARS-CoV2 in situ RNA data, serial sections of the lung tissues and additional nasopharyngeal swabs were tested for the viral proteins spike (S1 and S2 subunits separately) and nucleocapsid by immunohistochemistry. Representative data is provided in Fig. 1C–F. Note that the viral RNA and the SARS-CoV2 specific proteins showed the same distribution in the viral positive lung samples and each were negative, or showed rare positive cells, in the COVID-19 lungs with no or low SARS-CoV2 copy number (data not shown).

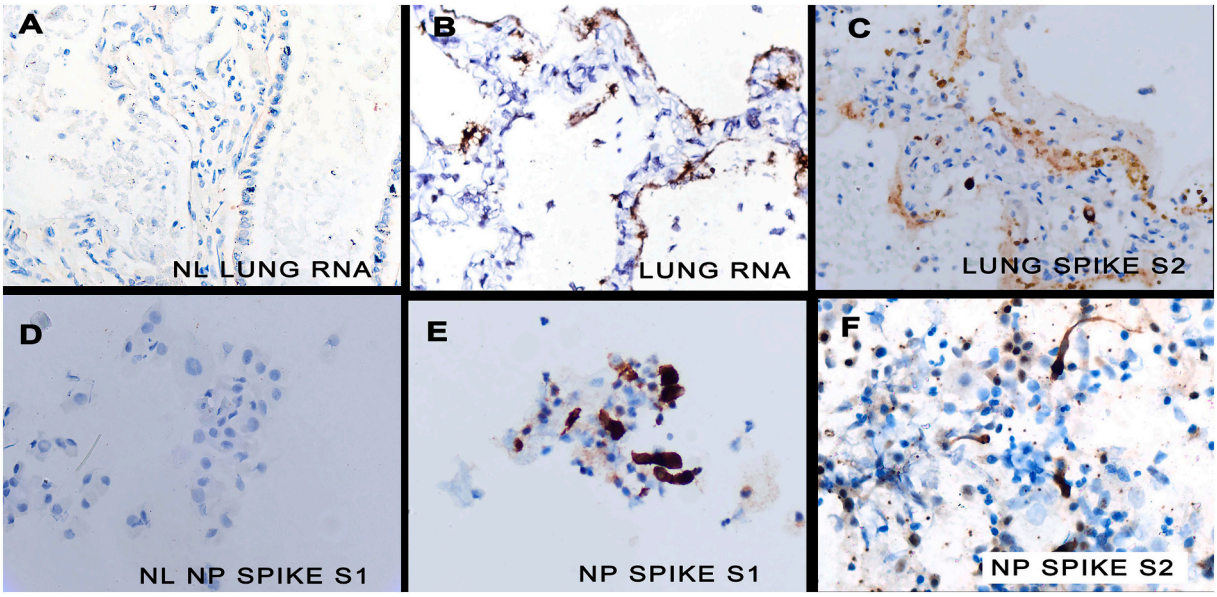

Fig. 1. Viral findings in mild versus severe SARS-CoV2 infection. The control lungs showed no viral protein or RNA (panel A) whereas the lung tissue from someone who died of COVID-19 showed high viral RNA (panel B) and the spike protein subunit 2 (panel C) in the same alveolar wall distribution. Similarly, note the absence of the viral spike protein in the uninfected nasopharynx swab (panel D) and the strong signal for spike subunit 1 (panel E) and spike subunit 2 proteins (panel F) in glandular cells from a person with mild disease. NP – nasopharyngeal, NL – normal control, and the signal is brown due to DAB with hematoxylin counterstain. (For interpretation of the references to color in this figure legend, the reader is referred to the web version of this article.)

Similarly, SARS-CoV2 nucleocapsid and spike proteins were detected by immunohistochemistry in each of the twenty viral positive nasopharyngeal swabs and in none of the controls. The viral proteins were detected only in the glandular cells in percentages equivalent to the viral RNA and each other (Fig. 1E, F).

3.4. Immunohistochemistry for the immune response in the nasopharyngeal swabs and the COVID-19 autopsy lungs

Having established that the viral positive nasopharyngeal swabs and ten COVID-19 lung samples each showed a strong productive infection, defined as equivalent and large amounts of viral RNA and proteins in the specimen, the samples were next tested to determine the numbers and distribution of various classes of lymphocytes (CD3, CD8, CD20, FOXP3), macrophages (CD11b, CD163, and CD206), neutrophil count, and PDL1 response, since the latter is a typical marker of productive viral infection [19]. These analyses were done concurrently with the normal, viral negative controls and the data was generated blinded to the viral results and clinical information.

The nasopharyngeal data is compiled in Table 1. Note that there was no change in the number of B cells (CD20), T regulatory cells (FOXP3) or neutrophils in the control versus SARS-CoV2 infected nasopharyngeal samples. There was a marked and highly significant increase in the number of CD3 T cells and macrophages as evidenced by CD11b, CD163, and CD206 as well as PDL1 expression ($p < 0.001$). Analysis of these samples for CD8 did confirm that over 75 % of the CD3+ cells were cytotoxic T cells (data not shown).

Next, the same analyses were done for the COVID-19 lung samples compared to the controls (Table 2). Note that, there was no change in the number of B cells (CD20), T regulatory cells (FOXP3), CD3 cells, or neutrophils in the control versus SARS-CoV2 high copy number lung samples. There was a marked and highly significant increase in the number of macrophages as evidenced by CD11b, CD163, and CD206 plus much increased PDL1 expression compared to the controls.

As seen in Table 2, the same data was generated for the COVID-19 lungs which were not SARS-CoV2 associated. Note that when compared to the controls, these viral negative/low copy COVID-19 lungs showed a significantly increased CD3 count and CD163 count. Interestingly, when comparing the COVID-19 lungs with low/no virus versus the samples with high viral load, the former, besides showing the marked increase CD3 count, also showed a significant reduction in the CD11b, CD206, and PDL1 levels. Analysis of these samples for CD8 did confirm that over 75 % of the CD3+ cells were cytotoxic T cells (data not shown).

Fig. 2 plots the fold increase in the different lymphocyte and macrophage markers as well as PDL1 in the samples versus the controls. Note that the response for each immune marker was the strongest in the mild infections, that CD11b and CD206 were each increased with the viral infection, but much more so in the mild infections, and that equivalent results were evident in the mild versus fatal infection with high viral load for CD163 and PDL1.

Representative examples of the differential immune response in both

Table 1
Compilation of the immune response to mild infection in the nasopharyngeal swabs.[a]

Category	CD3[b]	CD20	FOXP3	CD11b	CD163	CD206	PDL1	Neutrophil	SARS-CoV2 spike[c]
Controls N = 20	**0.3 (0.1)**	0.1 (0.1)	0.2 (0.1)	**3.9 (0.7)**	**0.4 (0.1)**	**0.6 (0.2)**	**2.1 (0.8)**	1.4 (0.5)	**0**
SARS-CoV2 positive N = 20	**7.2 (1.1)** **p < 0.001**	0.1 (0.1)	0.1 (0.1)	**44.2 (5.3)** **p < 0.001**	**5.1 (1.2)** **p < 0.001**	**5.5 (2.0)** **p < 0.001**	**44.7 (7.1)** **p < 0.001**	2.1 (0.5)	**16.2 (3.8)** **p < 0.001**

[a] The data is presented as the percentage of total cells (mean/SEM).
[b] All data with a significant increase in the viral positive compared to the controls is shown in bold.
[c] Equivalent data was generated after testing for viral RNA and nucleocapsid proteins.

Table 2
Compilation of the immune response to fatal infection in the COVID-lungs.[a]

Category	CD3[b]	CD20	FOXP3	CD11b	CD163	CD206	PDL1	Neutrophil
Controls N = 10	0.2 (0.1)	0.1 (0.1)	0.2 (0.1)	**4.9 (1.1)**	**3.3 (0.9)**	**5.1 (1.3)**	**2.2 (1.0)**	0.1 (0.1)
SARS-CoV2 high viral number N = 10	0.4 (0.1)	0.1 (0.1)	0.3 (0.1)	**26.3 (4.2) p < 0.001**	**32.2 (5.1) p < 0.001**	**17.9 (3.9) p < 0.001**	**42.5 (5.1) p < 0.001**	0.4 (0.2)
SARS-CoV2 not virus associated[c] N = 10	**4.4 (1.7) p < 0.001**	0.1 (0.1)	0.3 (0.1)	**10.3 (2.9) p = 0.004**	**28.1 (5.0) p < 0.001**	5.3 (2.2)	**26.9 (7.0) p < 0.001**	0.5 (0.3)

[a] The data is presented as the percentage of total cells (mean/SEM).
[b] All data with a significant increase in the SARS-CoV2 lung samples compared to the controls are shown in bold.
[c] When comparing the COVID-19 lung tissues that were viral negative versus high viral load, there was a significant increase in the former for the CD3 count and a significant decrease in the CD11b, CD206 and PDL1 counts (each at p = 0.001).

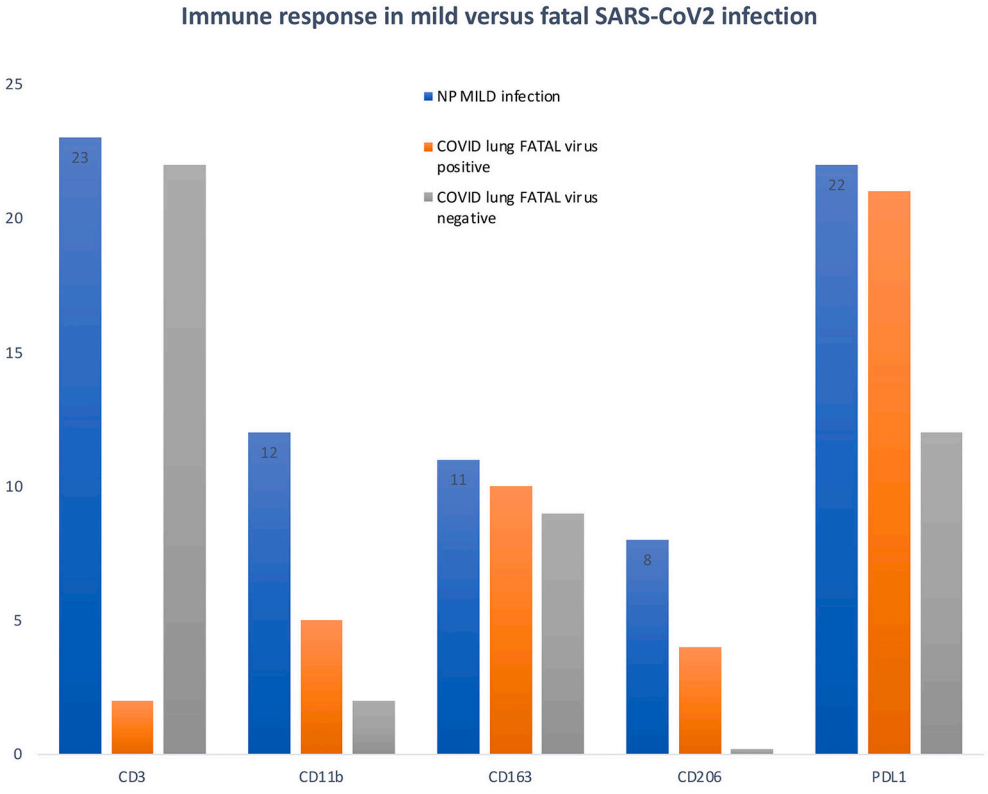

Fig. 2. Immune response in mild versus fatal SARS-CoV2 infection.
The figure shows a graphic representation of the fold changes from baseline in the nasopharyngeal swabs positive for SARS-CoV2 (blue columns) as well as the lung tissues from fatal COVID-19 that either had very high copy SARS-CoV2 (orange columns) or were not associated with SARS-CoV2 infection (gray columns). (For interpretation of the references to color in this figure legend, the reader is referred to the web version of this article.)

the nasopharynx and lung are provided in Fig. 3. Note the lack of a CD3 response in normal nasopharyngeal swabs (Fig. 3A) versus increased CD3 cells in the viral positive swabs from mildly infected people (Fig. 3B), the lack of a PDL1 response in normal nasopharyngeal swabs (Fig. 3C) versus a strong PDL1 response in the viral positive swabs from mildly infected people (Fig. 3D). Also note the strong CD8 presence in the fatal COVID-19 lung not viral associated (Fig. 3E) versus the lack of CD8 cells in the fatal COVID-19 lung with a high SARS-CoV2 presence (Fig. 3F).

3.5. Immunohistochemistry for hypercoagulable state and complement activation in the COVID-19 autopsy lungs

Fatal COVID-19 has been associated with increased Complement 5b-9 activation and a hypercoagulable state [6]. To determine if this was due directly to viral infection, or represented a systemic effect, the twenty lung tissues were examined by immunohistochemistry for complement component 6, CD41 (a marker of platelet activation), and, in selected cases, fibrinogen. Each of the ten lung samples from fatal COVID-19 that had high SARS-CoV2 viral load showed strong complement 6 expression involving over 33 % of the lung area. Complement component 6, as well as fibrinogen, had had the same distribution as the viral RNA and spike/nucleocapsid proteins and was most prominent in the alveolar capillary septa in either pneumocytes or endothelia (Fig. 4C and D arrows, respectively with Fig. 4A being a negative control). Co-localization experiments confirmed that the viral spike protein and RNA each showed a strong co-expression with C5b-9 as shown previously [6] and complement component 6 (data not shown), Of the ten COVID-19 lungs with little/no SARS-CoV2 infection, 5/10 showed complement component 6 expression and it was rare in that it involved <5 % of the total lung area (Fig. 4B).

With regards to CD41, none of the controls showed a signal (Fig. 4E) whereas18/20 (90 %) of the COVID-19 lungs showed a signal that localized mostly in the lumens of arterioles and venules. Note in Fig. 4F that CD41 was found in both the arterioles/venules and alveolar septa (arrow) in the lungs with high viral copy number (10/10 cases were positive); fibrinogen had a similar pattern (data not shown). However, in the fatal COVID-19 lungs not associated with SARS-CoV2, 8/10 (80 %) of the cases were positive for CD41 but the signal localized to just the smaller vessels and not the alveolar septa (Fig. 4G).

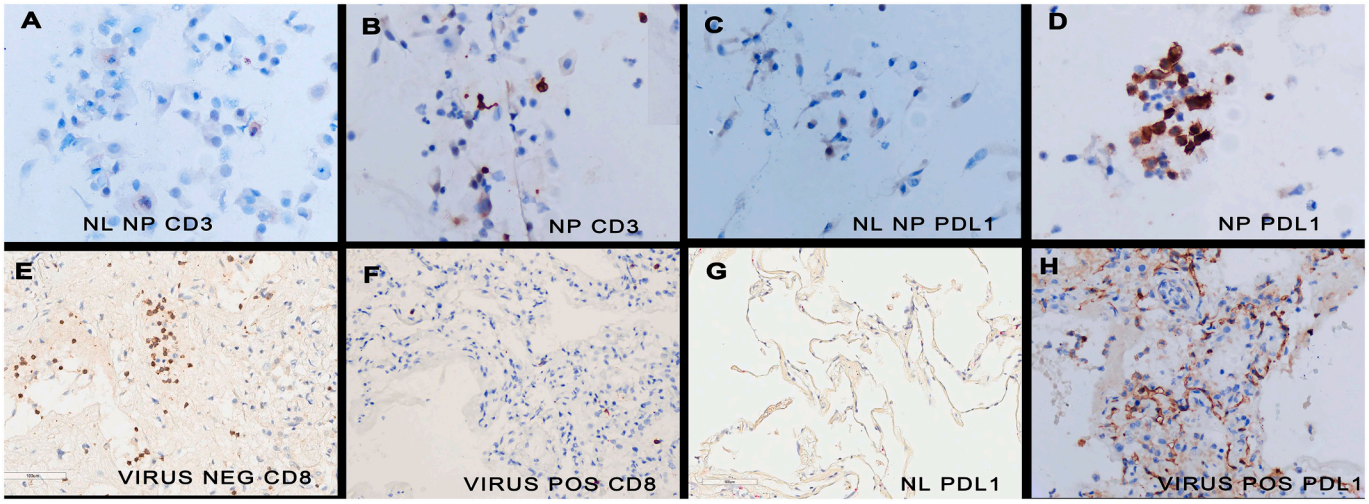

Fig. 3. In situ demonstration of the immune response in mild versus fatal SARS-CoV2 infection. Note the absence of a CD3 response in the uninfected nasopharynx swab (panel A) and the strong infiltration by these cells in an infected swab from a person with mild disease (panel B). Similarly, the control nasopharynx sample shows no PDL1 expression (panel C) whereas the infected nasopharynx shows a strong PDL1 response (panel D). Note that the lung from a fatal COVID-19 case not associated with viral infection did show a strong CD8 response (panel E) whereas this lung tissue from someone who died of COVID-19 that was strongly positive for SARS-CoV2 did not show a CD8 response (panel F). The control lungs showed a very weak PDL1 signal (panel G) whereas the COVID-19 lungs with high viral copy number did show strong PDL1 expression (panel H). NP – nasopharyngeal, NL – normal control, and the signal is brown due to DAB with hematoxylin counterstain. (For interpretation of the references to color in this figure legend, the reader is referred to the web version of this article.)

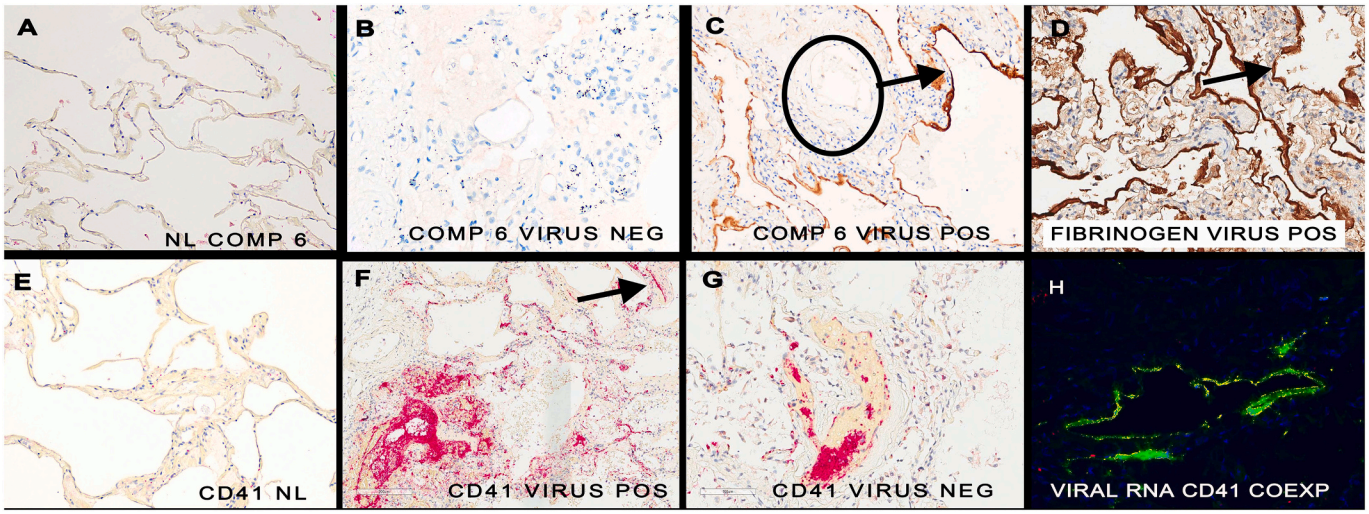

Fig. 4. In situ demonstration of the clotting and complement activation in the fatal COVID-19 lungs. Note the absence of complement component 6 in the normal lung (panel A) as well as the lung from a fatal COVID-19 case that did not contain detectable SARS-CoV2 RNA (panel B). Panel C shows that the signal for complement component 6 in the COVID-19 lung tissue associated with high SARS-CoV2 copy number localizes only to the alveolar septa (arrows) which also shows a strong signal for fibrinogen (panel D); no signal is evident in the small vessels (oval). Panel E shows the lack of signal for CD41 in the normal lung controls. In comparison, note the CD41+ platelet aggregates in the small vessels in a lung from a person who died of COVID-19 associated with high viral copy number (panel F) as well as from the same lung that was not associated with SARS-CoV2 infection (panel G). However, note that the CD41 signal localizes only to the alveolar septa in the lung with high copy SARS-CoV2 (arrow, panel F). Co-localization of CD41 (fluorescent red) with SARS-CoV2 RNA (fluorescent green) documents that CD41 strongly co-expressed with the viral RNA in the lung samples with high copy viral RNA (seen as fluorescent yellow, panel H). NL – normal control, and the signal in panels A–D is brown due to DAB and fast red in panels E–G with hematoxylin counterstain.
(For interpretation of the references to color in this figure legend, the reader is referred to the web version of this article.)

3.6. Histologic findings in the COVID-19 lungs relative to the presence of SARS-CoV2 productive viral infection

Lastly, H&Es from the twenty fatal COVID-19 lung tissues were examined blinded to the viral findings. The following histologic variables were evaluated: diffuse alveolar damage, microhemorrhages, organizing pneumonia, bronchiolitis obliterans, bronchiolitis and/or chronic interstitial lymphocytic inflammation, plasmacytic inflammation, histiocytic dominant inflammation, vascular endothelialitis, capillaritis, thrombosis (including microthrombi), and angiogenesis. A compilation of the data is presented in Fig. 5. Note that the two histologic features which were much more associated with the high copy SARS-CoV2 in the COVID-19 lungs were diffuse alveolar damage and thrombi, whereas the two features most associated with the "not viral associated" lungs were organizing pneumonia and bronchiolitis/chronic interstitial lymphocytic inflammation. Representative H&E findings are presented in Fig. 6 (nasopharyngeal swabs in panels A-C, fatal COVID-19 lung not viral associated in panels D–F, and fatal COVID-19 lung with

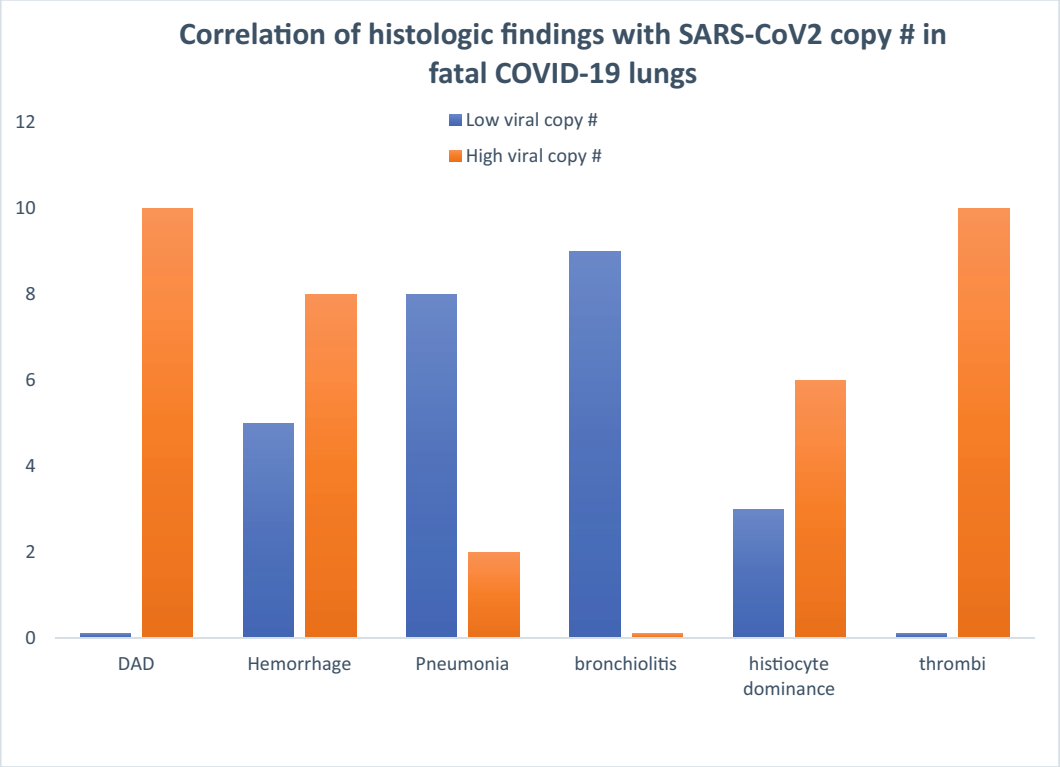

Fig. 5. Correlation of the H&E findings with the viral load in fatal COVID-19.
The figure shows a graphic representation of the histologic findings in the lung tissues from people who died of COVID-19 where there was high viral copy number (orange columns) and those not associated with direct SARS-CoV2 infection (blue columns). (For interpretation of the references to color in this figure legend, the reader is referred to the web version of this article.)

high SARS-CoV2 load in panels G-I).

4. Discussion

SARS-CoV2 is able to cause a massive productive infection, defined by abundant and equivalent distribution of viral RNA and proteins, in two sites: the nasopharynx and the lungs. The main focus of this study was to compare the immune response to the infection in these two areas focusing on people who had mild disease and recovered versus those who died of the disease. Viral in situ based testing did confirm that both the nasopharyngeal and lung samples contained abundant SARS-CoV2 marked by a high percentage of infected target cells that contained hundreds of viral genomes per cell and a corresponding large amount of the viral nucleocapsid and spike proteins. With regards to the immune response, both the mild and fatal infections showed equivalent elevated increases in PDL1 and the macrophage marker CD163 compared to controls. The immune response metric that most differentiated mild from fatal infection was the CD3/CD8 response, which was markedly greater in the mild infection. CD11b and CD206 counts were higher in the lung in fatal COVID-19 where there was abundant virus versus those COVID-19 lungs with no/low viral copy number relative to the controls. However, there was a significant increase in the macrophage markers CD11b and CD206 in mild versus fatal disease with high viral copy number suggesting their response may be reduced though not eliminated in the virus positive areas of the fatal disease. The relatively weak FOXP3 and CD20 response versus a robust PDL1 response to viral infection has been reported previously [19]. Both CD11b and CD206 have been shown to increase with severe COVID-19 [20-22] but this is based on peripheral blood mononuclear cell analyses and not in situ testing of the lung per se.

One possible explanation for the marked disparity in CD8 cell response in the productive infection in mild versus fatal disease, though unlikely, is that people with fatal disease had a systemic anergy-like response to most immunogens. However, the fatal COVID-19 lung areas with no or low copy virus showed a robust CD3/CD8 response. This suggests that in people with fatal COVID-19 the virus is able to directly block the signaling that allows CD3/CD8 cells to infiltrate the infected tissue. Another possibility is that the microthrombi so prevalent in the alveolar capillaries in fatal COVID-19 lung with abundant SARS-CoV2 may physically block a cytotoxic T cell response. Further study will be needed to clarify the mechanisms of this process, but the data strongly suggests that the muted CD8 response in fatal COVID-19 is not due to PDL1 overexpression which was equivalent in the mild and fatal cases. The mechanism may be linked to obesity and diabetes mellitus type 2, since these are so strongly correlated with the risk of severe/fatal disease in COVID-19. Indeed, reduced T cell functioning has been associated with obesity and diabetes [23,24]. However, to underscore the complexity of the topic, in other infectious diseases of the lung, such as influenza A, obesity has been related to a hyper-immune response to the viral infection that leads to increased lung damage and a much increased cytokine storm [25].

A review of the histology of the fatal COVID-19 lungs from the tissues with high viral copy and low/no viral RNA gives important clues about the pathophysiology of severe COVID-19. In the lung samples with abundant SARS-CoV2 infection, the main pathologic findings are typical of acute lung injury. There is diffuse alveolar damage and many areas with microthrombi. This was originally described by Magro et al as a microangiopathy in which viral RNA, nucleocapsid, and spike proteins co-express with C5b-9, induce microthrombi, and lead to the death of the cells in the alveolar capillary linings [6]. We noted the same molecular findings in this study, and demonstrated that complement component 6, fibrinogen, and platelets are all part of the microthrombi that form in the lungs in fatal COVID-19 in response to the productive viral infection. Interestingly the lung tissues from people who died of

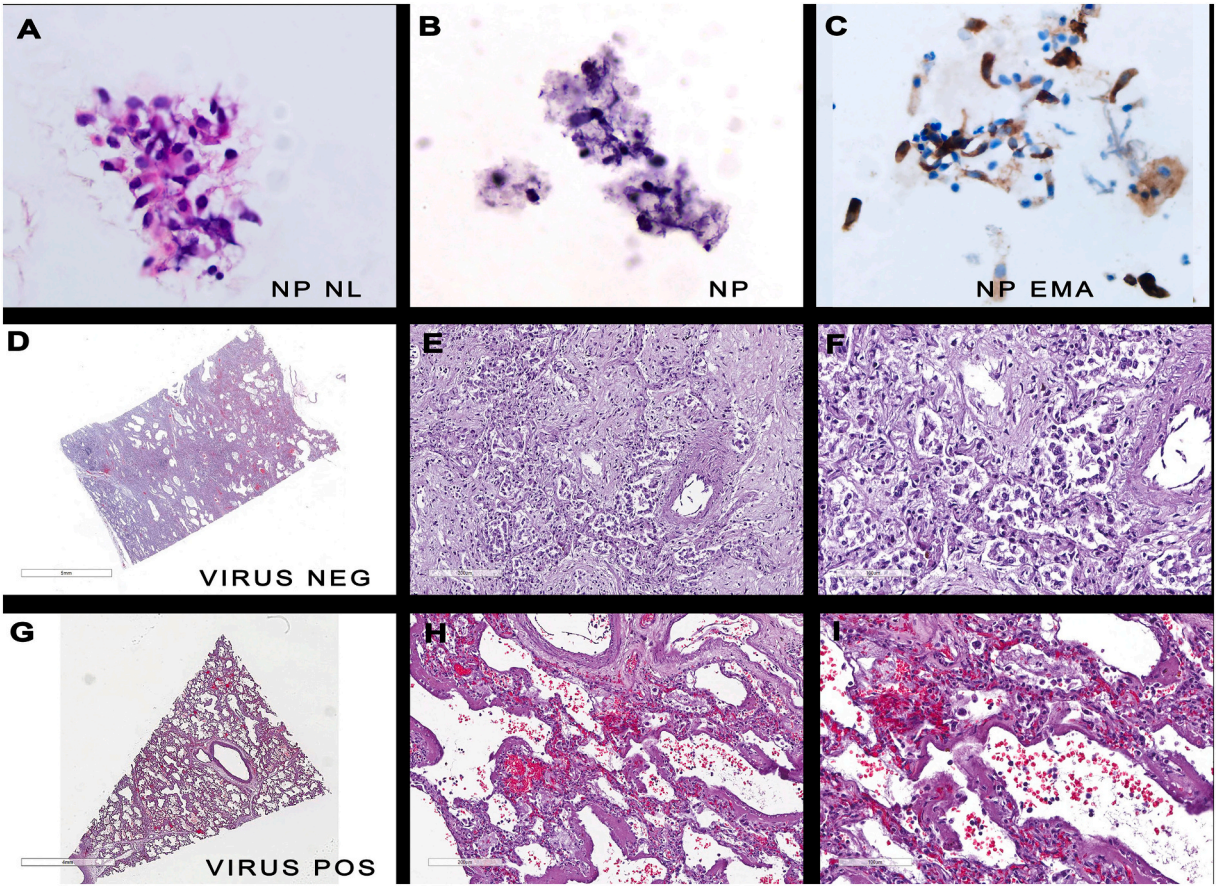

Fig. 6. H&E findings of mild versus fatal SARS-CoV2 infection. Panels A–C compare the cytologic findings in the normal nasopharynx (panel A) and mild infection (panel B); note that the glandular cells show degenerative changes that is highlighted with the EMA immunohistochemistry test (panel C). Panels D–F show successively high magnifications in a lung from a person who died of COVID-19 in which viral RNA was not evident; note the presence of extensive organizing pneumonia with scattered chronic inflammatory infiltrates. Panels G-I show successively high magnifications in a lung from a person who died of COVID-19 with high copy viral RNA; note the diffuse alveolar damage characterized by hyaline membrane formation, hemorrhage, and destruction of lining pneumocytes.

COVID-19 but where there was no or little virus showed a more chronic phase of disease that included organizing pneumonia with a robust lymphocyte presence as well as bronchiolitis and/or chronic interstitial lymphocytic inflammation. These findings are similar to that described by Felix et al. [26] who described acute and chronic lung disease in fatal COVID-19. The alveolar septal wall cell inhabitants (endothelial cells and pneumocytes) were readily apparent in the chronic disease as compared to the microangiopathy where they were nearly obliterated. Although it is acknowledged that areas of organization may represent healing of prior areas of acute injury, it is tenable that the chronic phase of the lung disease may encompass areas of the lung areas not involved by the initial productive infection and may represent changes induced by cytokines and other systemic manifestations of fatal COVID-19, especially since evidence of microangiopathy was not evident in the viral negative lung sections. In this regard, a surprising finding of this study was that platelet aggregates in arterioles and venules, but not in the alveolar wall septa, as defined by CD41 immunohistochemistry testing, were present in 80 % of the lung samples that lacked high copy SARS-CoV2, despite the absence of the unequivocal microthrombi seen with H&E. This suggests that the hypercoagulable state typical of fatal COVID-19, and reflecting systemic complement activation [6], may be responsible for the platelet aggregation as seen in the lungs in this study.

A limitation of this study is that it compared productive infection in two different sites: nasopharynx (mild) and lung (fatal). Clearly, lung tissue is not available in people with mild symptoms. Our conclusions are based in part on the hypothesis that the immune response to the virus in the nasopharynx is comparable to that in the lung. Nasopharyngeal samples from people who died of the disease could help address this question but were not available for this study. Still, both the lung and nasopharynx showed high viral copy infections in the mild and severe disease, as defined by the number of infected cells and the signal intensity of the in situ based test [27] which suggests that a comparison of the data would yield useful information.

In sum, the data suggests that both mild and severe infection share marked viral proliferation but that in the former there is a much more robust cytotoxic T cell response as well as macrophage response. Also, the lung in fatal COVID-19 will show markedly different histologic findings based on the amount of SARS-CoV2 present in a given section, which can vary in a given person which underscores the value of ample sectioning of the lungs in fatal COVID-19. The H&E findings of diffuse alveolar damage and microthrombi strongly suggest active, marked productive viral infection whereas the lack of these findings with the presence of an organizing pneumonia and bronchiolitis and/or chronic interstitial lymphocytic inflammation suggests a systemic effect typical of the fatal disease. The basis for the reduced cytotoxic T cell/macrophage response in the lung with fatal productive viral infection may involve mechanisms induced by obesity and/or diabetes as most of the patients in this study who died of the disease had these pre-existing conditions.

Declaration of competing interest

The authors have no conflict of interests to report.

Acknowledgments

The authors greatly appreciate the help of Dr. Margaret Nuovo with the photomicroscopy, Dr. Saul Suster and Dr. Cynthia Magro who provided samples and much advice/comments and Ms. Eva Matys who performed the histotechnical work.

References

[1] Gautret P, Million M, Jarrot PA, et al. Natural history of COVID-19 and therapeutic options. Dec Expert Rev Clin Immunol 2020;16(12):1159–84. https://doi.org/10.1080/1744666X.2021.1847640. Epub 2020 Dec 24. PMID: 33356661.

[2] Machhi J, Herskovitz J, Senan AM, et al. The natural history, pathobiology, and clinical manifestations of SARS-CoV-2 infections. J Neuroimmune Pharmacol 2020 Sep;15(3):359–86. https://doi.org/10.1007/s11481-020-09944-5. Epub 2020 Jul 21. PMID:.

[3] Toor SM, Saleh R, Sasidharan Nair V, Taha RZ, Elkord E. T-cell responses and therapies against SARS-CoV-2 infection. Immunology 2021 Jan;162(1):30–43. https://doi.org/10.1111/imm.13262. Epub 2020 Oct 27. PMID: 32935333; PMCID: PMC7730020.

[4] Wang J, Jiang M, Chen X, Montaner LJ. Cytokine storm and leukocyte changes in mild versus severe SARS-CoV-2 infection: Review of 3939 COVID-19 patients in China and emerging pathogenesis and therapy concepts. J Leukoc Biol 2020 Jul; 108(1):17–41. https://doi.org/10.1002/JLB.3COVR0520-272R. Epub 2020 Jun 13. PMID: 32534467; PMCID: PMC7323250.

[5] Neidleman J, Luo X, George AF, et al. Distinctive features of SARS-CoV-2-specific T cells predict recovery from severe COVID-19. Cell Rep 2021 Jul 20;36(3):109414. https://doi.org/10.1016/j.celrep.2021.109414. Epub 2021 Jun 29. PMID: 34260965; PMCID: PMC8238659.

[6] Magro C, Mulvey JJ, Berlin D, Nuovo G, Salvatore S, Harp J, Baxter-Stoltzfus A, Laurence J. Complement associated microvascular injury and thrombosis in the pathogenesis of severe COVID-19 infection: a report of five cases. Transl Res 2020 Jun;220:1–13. https://doi.org/10.1016/j.trsl.2020.04.007. Epub 2020 Apr 15. PMID: 32299776; PMCID: PMC7158248.

[7] Nuovo GJ, Magro C, Shaffer T, Awad H, Suster D, Mikhail S, He B, Michaille JJ, Liechty B, Tili E. Endothelial cell damage is the central part of COVID-19 and a mouse model induced by injection of the S1 subunit of the spike protein. Ann Diagn Pathol 2021 Apr;51:151682. https://doi.org/10.1016/j.anndiagpath.2020.151682. Epub 2020 Dec 24. PMID: 33360731; PMCID: PMC7758180.

[8] Nuovo GJ, Magro C, Mikhail A. Cytologic and molecular correlates of SARS-CoV-2 infection of the nasopharynx. Ann Diagn Pathol 2020 Oct;48:151565. https://doi.org/10.1016/j.anndiagpath.2020.151565. Epub 2020 Jun 13. PMID: 32534467; PMCID: PMC7323250.

[9] Zhang Y, Geng X, Tan Y, et al. New understanding of the damage of SARS-CoV-2 infection outside the respiratory system. Biomed Pharmacother 2020;127:110195. https://doi.org/10.1016/j.biopha.2020.110195.

[10] Li H, Liu L, Zhang D, et al. SARS-CoV-2 and viral sepsis: observations and hypotheses. Lancet 2020;395(10235):1517–20. https://doi.org/10.1016/S0140-6736(20)30920-X.

[11] Zhou L, Zhang M, Wang J, Gao J. Sars-Cov-2: underestimated damage to nervous system. Travel Med Infect Dis 2020;36:101642. https://doi.org/10.1016/j.tmaid.2020.101642.

[12] Varga Z, Flammer AJ, Steiger P, Haberecker M, Andermatt R, Zinkernagel A, Mehra M, Schuepbach R, Ruschitzha F, Moch H. TEndothelial cell infection and endotheliitis in COVID-19. The Lancet. https://marlin-prod.literatumonline.com/pb-assets/Lancet/pdfs/S0140673620309375.pdf.

[13] Avolio E, Carrabba M, Milligan R, et al. The SARS-CoV-2 spike protein disrupts human cardiac pericytes function through CD147 receptor-mediated signalling: a potential non-infective mechanism of COVID-19 microvascular disease. Clin Sci (Lond) 2021 Dec 22;135(24):2667–89. https://doi.org/10.1042/CS20210735. PMID: 34807265; PMCID: PMC8674568.

[14] Frank MG, Nguyen KH, Ball JB, Hopkins S, Kelley T, Baratta MV, Fleshner M, Maier SF. SARS-CoV-2 spike S1 subunit induces neuroinflammatory, microglial and behavioral sickness responses: Evidence of PAMP-like properties. Brain Behav Immun 2022 Feb;100:267–77. https://doi.org/10.1016/j.bbi.2021.12.007. Epub 2020 Jul 21. PMID:.

[15] Gu T, Zhao S, Jin G, et al. Cytokine signature induced by SARS-CoV-2 spike protein in a mouse model. Front Immunol 2021 Jan;28(11):621441. https://doi.org/10.3389/fimmu.2020.621441. PMID: 33584719; PMCID: PMC7876321.

[16] Nuovo GJ, Suster D, Tili E, Awad H, Magro C. A standardized protocol for the in situ detection of SARS-CoV2 RNA and proteins. Appl Immunohistochem Mol Morphol 2021. https://doi.org/10.1097/PAI.0000000000000992. on line.

[17] Nuovo GJ, Suster D, Awad H, Michaille JJ, Tili E. The histologic and molecular correlates of liver disease in fatal COVID-19 including with alcohol use disorder. Ann Diagn Pathol 2021 Dec 23;57:151881. https://doi.org/10.1016/j.anndiagpath.2021.15188. Epub ahead of print. PMID: 34968863; PMCID: PMC8694815.

[18] Nuovo G. False-positive results in diagnostic immunohistochemistry are related to horseradish peroxidase conjugates in commercially available assays. Ann Diagn Pathol 2016 Dec;25:54–9. https://doi.org/10.1016/j.anndiagpath.2016.09.010. Epub 2016 Sep 26 PMID: 27806847.

[19] Mezache L, Magro C, Hofmeister C, Pichiorri F, Sborov D, Nuovo GJ. Modulation of PD-L1 and CD8 activity in idiopathic and infectious chronic inflammatory conditions. Appl Immunohistochem Mol Morphol 2017 Feb;25(2):100–9. https://doi.org/10.1097/PAI.0000000000000298. PMID: 27438510; PMCID: PMC5247427.

[20] Gao C, Zeng J, Jia N, et al. SARS-CoV-2 Spike Protein Interacts With Multiple Innate Immune Receptors. 2020.07.29.227462. bioRxiv [Preprint]; 2020 Jul 30. https://doi.org/10.1101/2020.07.29.227462. PMID: 32766577; PMCID: PMC7402034.

[21] Trombetta AC, Farias GB, Gomes AMC, et al. Severe COVID-19 recovery is associated with timely acquisition of a myeloid cell immune-regulatory phenotype. Front Immunol 2021 Jun;23(12):691725. https://doi.org/10.3389/fimmu.2021.691725. PMID: 34248984; PMCID: PMC8265310.

[22] Karawajczyk M, Douhan Håkansson L, Lipcsey M, Hultström M, Pauksens K, Frithiof R, Larsson A. High expression of neutrophil and monocyte CD64 with simultaneous lack of upregulation of adhesion receptors CD11b, CD162, CD15, CD65 on neutrophils in severe COVID-19. Ther Adv Infect Dis 2021 Jul;31(8): 20499361211034065. https://doi.org/10.1177/20499361211034065. PMID: 34377464; PMCID: PMC8326822.

[23] Green WD, Beck MA. Obesity altered T cell metabolism and the response to infection. Curr Opin Immunol 2017 Jun;46:1–7. https://doi.org/10.1016/j.coi.2017.03.008. Epub 2017 Mar 27. PMID: 28359913; PMCID: PMC5554716.

[24] Karlsson EA, Sheridan PA, Beck MA. Diet-induced obesity impairs the T cell memory response to influenza virus infection. J Immunol 2010 Mar 15;184(6): 3127–33. https://doi.org/10.4049/jimmunol.0903220. Epub 2010 Feb 19 PMID: 20173021.

[25] Zhang AJ, To KK, Li C, et al. Leptin mediates the pathogenesis of severe 2009 pandemic influenza A(H1N1) infection associated with cytokine dysregulation in mice with diet-induced obesity. J Infect Dis 2013 Apr 15;207(8):1270–80. https://doi.org/10.1093/infdis/jit031. Epub 2013 Jan 16 PMID: 23325916.

[26] Felix JC, Sheinin YM, Suster D, et al. Diffuse interstitial pneumonia-like/macrophage activation syndrome-like changes in patients with COVID-19 correlate with length of illness. Ann Diagn Pathol 2021 Aug;53:151744. https://doi.org/10.1016/j.anndiagpath.2021.151744. Epub 2021 Apr 19. PMID: 33991784; PMCID: PMC8053602.

[27] Nuovo GJ. In situ molecular pathology and co-expression analyses. 2nd edition. San Diego CA: Elsevier; Sept 2020.